RESEARCH

Natural leather based gamma-ray shielding materials enabled by the coordination of well-dispersed Bi^{3+}/Ba^{2+} ions and RE_2O_3 coating

Yue Shen[1,2], Jibo Zhou[1,2], Zheng Han[3], Hao Li[1,2], Linping Yan[1,2], Xuepin Liao[1,2]* and Bi Shi[1,2]

Abstract

Gamma rays is widely used in modern science and technology, but it may cause health damage to practitioners. In the present study, natural composites based on leather and high-Z elements (atomic number $\geq$ 56) were fabricated and used as gamma rays shielding materials. These shielding materials were prepared by coating rare earth nanoparticles (Er_2O_3 or La_2O_3) onto the surface of natural leather, which was first impregnated with Bi^{3+} and Ba^{2+}. Results show that the attenuation efficiency of the prepared $Er_{1.31}Bi_{5.46}$-NL (1.31 and 5.46 mmol cm^{-3} loaded elements) with thickness of 3.2 mm was 61.57% for incident rays at 121.78 keV (^{152}Eu) and reached 96.4% in the incident of 59.5 keV (^{241}Am), which is comparable to that of 0.25-mm lead plate (54.54 mmol cm^{-3}). In addition, these natural-leather-based shielding materials exhibited low density (approximately 1/10 of Pb), high strength and wearable behaviors.

Keywords: Gamma rays, Natural leather, High-Z elements, Rare earth elements, Nanoparticles, Wearability, Attenuation efficiency

Graphical abstract

*Correspondence: xpliao@scu.edu.cn
[1] Department of Biomass Science and Engineering, Chengdu 610065, China
Full list of author information is available at the end of the article

Shen *et al. Journal of Leather Science and Engineering*   (2022) 4:15

Page 2 of 11
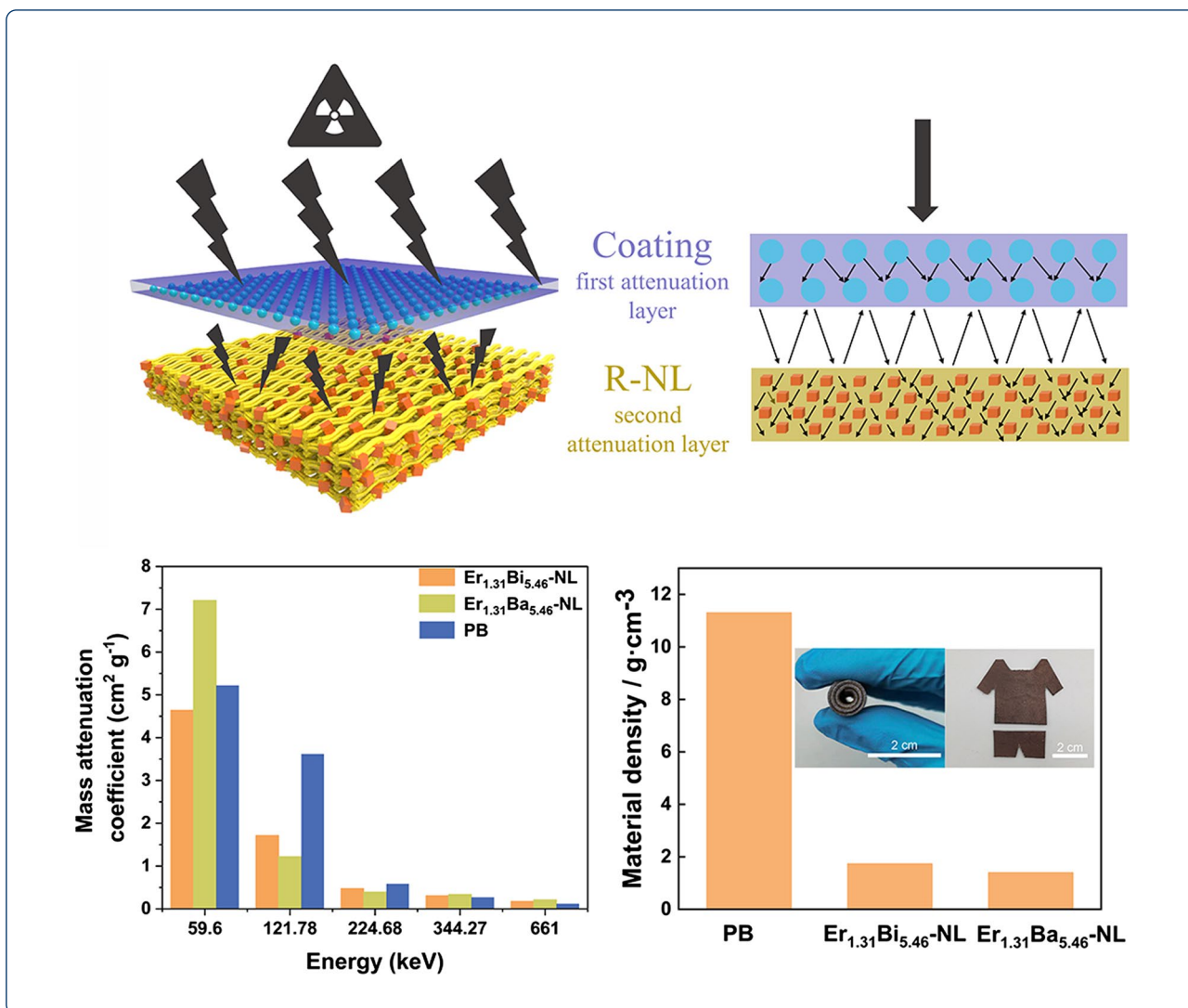
1 Introduction

In recent years, gamma rays have been widely used in different fields, such as industrial flaw detection [1], medical imaging [2] and radiotherapy [3]. However, its leakage may cause potential harm to human beings. Ions produced by gamma-ray ionization can destroy many human cellular macromolecules such as DNA, lipids, and proteins, causing a series of serious diseases [4]. Therefore, ray radiation protection materials with satisfied shielding performance should be developed for the safety utilization of gamma rays.

The photoelectric effect (for $E_\gamma < 400$ keV, E_γ photon energy), Compton scattering (for 400 keV $< E_\gamma < 1.022$ MeV), and pair production (for $E_\gamma > 1.022$ MeV), which are the main interactions between gamma rays and substance, transfer part or all of the energy from photons to electrons [5]. Apart from the energy of incident gamma rays, the attenuation performance of the material is related to the atomic number and dosage of high Z elements [6–8]. A high-Z element (atomic number > 56) is likely to interact with incident gamma photons to produce photoelectric effect, because the tighter electrons are bound by the atom, making it easier for the nucleus to participate in the photoelectric process to meet the requirements of energy and momentum conservation. The photoelectric effect (σ_{ph}) is greatly related with atomic number of substance and gamma photons energy ($\sigma_{ph} \propto \frac{Z^4}{h\upsilon}$). The Compton effect occurs between gamma photons and free electrons, and the Compton scattering cross section (σ_c, the probability of Compton scattering between matter and gamma photons) is related to the atomic number of the substance and gamma photons energy ($\sigma_c \propto \frac{Z}{h\upsilon}$). Therefore, the energy of gamma photons can be well attenuated when the high-Z element is

incorporated into materials. Traditionally, concrete [9, 10], lead glass [11, 12], and other materials containing heavy elements are applied to shield gamma rays, and they have the advantages of easy availability of raw materials and low cost. However, these materials are too heavy to be transported and cannot be used for the protection of moving targets. Lead is commonly used as shielding materials because its high density ($\rho = 11.3$ g cm^{-3}) and high atomic number ($Z = 82$), but lead has biologically toxicity and has weak absorption area (40–80 keV) [13]. To prepare shielding materials for the moving targets, researchers conducted extensive research and development of flexible materials. Ahmed et al. incorporated 88.1 wt.% of micro tungsten powder with silicone by a room temperature vulcanized method to prepare flexible silicone/tungsten, and the mass attenuation coefficient was 0.1035 cm^2 g^{-1} in the incident of 661 keV [14]. Canel et al. prepared an epoxy resin containing iron, bismuth, tantalum, and tungsten carbide for gamma rays shielding [15], and the linear attenuation coefficient of tungsten-powder-filled epoxy resin was 0.27 cm^{-1} for ^{60}Co.

Natural leather is a wearable material with three-dimensional fiber network woven structure. Three polypeptide chains (called α chains) make up the collagen molecule, which is the basic building block of natural leather. Collagen molecules further form collagen fiber, collagen fiber bundle, and eventually a multi-level structure of fibrous network [16, 17]. In addition, various active groups on collagen molecules (e.g., –COOH and –NH$_2$) result in the excellent feature of natural leather to bond with many meatal ions [18]. Therefore, high-Z elements will be uniformly bonded with natural leather. Considering its multi-level structure of fibrous network, the photons will undergo multiple collisions with high-Z elements in natural leather, thus enhancing the photons energy attenuation, and resulting in the excellent shielding performances for the gamma rays.

In the present work, we designed a multilayered high-performance gamma-ray shielding material (RZ-NL) based on natural leather. For the preparation of RZ-NL, natural leather was first impregned with high-Z metal ions (Z-NL), and further coated with rare earth nanoparticles (RZ-NL) to enhance the gamma-ray attenuation ability. When gamma photons pass through the prepared shielding material, rare earth elements in the coating layer will first collide with the gamma photons and decay their energy, and then Z-NL acts as a second attenuation layer to further reduce photons energy. Accordingly, wearable materials with outstanding gamma-ray attenuation performance shielding materials will be obtained.

2 Experimental section

2.1 Materials

Ammonium bismuth citrate (99%, Bi$_X$(NH$_3$)$_X$C$_6$H$_7$O$_7$), barium acetate (99%, (CH$_3$COO)$_2$Ba), and tannic acid (95%, C$_{76}$H$_{52}$O$_{46}$) were provided by Aladdin Biochemical Technology Co., Ltd. Erbium oxide nanoparticles (99.99%, 50 nm, Er$_2$O$_3$) were obtained from Nanuo Technology Co., Ltd (Guangzhou, China), while lanthanum oxide nanoparticles (99.99%, 50 nm, La$_2$O$_3$) were obtained from Macklin Biochemical Co., Ltd (Shanghai, China). Acrylic resin (21–23 wt.%, RA K1901) was obtained from Dowell Science & Technology Co., Ltd (Sichuan, China). Chrome tanned leather (0.8 mm in thickness) was supplied by Ruixing Leather Co., Ltd (Zhejiang, China). The 0.25-mm lead plate was obtained from Xingye Metal Materials Co., Ltd (Zhejiang, China).

2.2 Sample preparation

The preparation process of RZ-NL was optimized as follows:

(1) Preparation of Z-NL. Z-NL was prepared by "equivalent-volume impregnation method". First, the pre-dehydrated chrome tanned leather (NL) was cut into 100 mm × 100 mm × 0.8 mm section, and then immersed in an equal volume solution containing 21.48 mmol Bi^{3+} and Ba^{2+}. After 2 h reaction, the Z-NL was obtained by air drying. Accordingly, a series of Z$_x$-NL containing different high-Z elements was prepared, where x was recorded as the amount of high-Z element loaded in NL (mmol cm^{-3}).

(2) Modification of rare earth nano particles (MRE$_2$O$_3$). A total of 20.91 mmol nano rare earth oxide particles (RE$_2$O$_3$) was added into a three-necked flask with 24 g ethanol (50 wt.%) and 2 g tannic acid, and then reacted at 80 °C for 3 h and MRE$_2$O$_3$ was obtained.

(3) Preparation of RZ-NL. The modified MRE$_2$O$_3$ was mixed with acrylic resin (2:1), and the mixture was spray-coated onto the surface of the prepared Z$_x$-NL, and R$_y$Z$_x$-NL containing different amounts of nano RE$_2$O$_3$ and high-Z element was prepared (y is the content of RE$_2$O$_3$ coated on natural leather, mmol cm^{-3}).

2.3 Characterization

The morphologies of NL, RE$_2$O$_3$, MRE$_2$O$_3$ and Z$_x$-NL were observed by FIB-SEM (Helios G4 UC) and the corresponding elemental mappings (Mappings) were obtained using the electron back scattering diffraction

Shen *et al. Journal of Leather Science and Engineering*   (2022) 4:15

Page 4 of 11

(EBSD) analysis system (Aztec, Thermo Fisher Scientific Inc., USA). The transmission electron microscope pattern images (TEM) of RE_2O_3 and MRE_2O_3 were obtained using Tecnai G2 F20 S-TWIN (Thermo Fisher Scientific Inc., USA). The stereoscope photos of RZ-NL were obtained by stereomicroscopic (CH-9435 Heerbrugg, Leica Microsystems Co. Ltd., Germany). The crystal morphology of metal elements was analyzed by X-ray diffraction (XRD, Bruker D8 advance, GE), and the pattern was recorded using a Cu source at a scanning speed of 8°/min. The density of the prepared materials was determined using a mercury injection pore analyzer (Micro-Active AutoPore V9600, Mike Instruments Inc., USA). Tensile strength (TS1) and tear strength (TS2) were be determined using a universal testing machine (AI-700 S, Gotech Machines Co. Ltd., China). The Fourier transform infrared (FTIR) pattern of the prepared sample was recorded via FTIR spectroscopy (Nicolet iS10, Thermo Fisher Scientific Inc., USA).

2.4 Gamma rays shielding performances
Gamma-ray generated by sources were detected using a low-background coaxial high-purity germanium detector (GEM30P4, ORTEC). Two standard point sources [241]Am and ^{137}Cs and a multi-gamma-ray source [152]Eu were used to test the attenuation efficiency (AE) of RZ-NL. Gamma photons with energies of 59.6 and 661 keV were generated using [241]Am and ^{137}Cs, respectively, while [152]Eu emits photons with energies of 121.78, 244.68 and 344.27 keV. RZ-NL was kept at the same height and 12 cm away from the gamma-ray source. Each sample was exposed to the gamma rays source for 500 s, and the dose accumulation was recorded and processed using GammaVision. Considering that the system error of GammaVision was very small and could be ignored at a test time of 500 s, we did not set the error value. The AE was calculated using the following formula:

$$AE = \frac{I_0 - I}{I_0} \times 100\%$$

where I_0 and I represent the counts of initial and penetrated gamma-ray at a given time, respectively.

The linear attenuation coefficient and mass attenuation coefficient can be calculated as follows:

$$I = I_0 e^{\mu d}$$

$$\mu_m = \frac{\mu}{\rho}$$

where μ is the linear attenuation coefficient and μ_m represents the mass attenuation coefficient, ρ is the density and d is the thickness of sample.

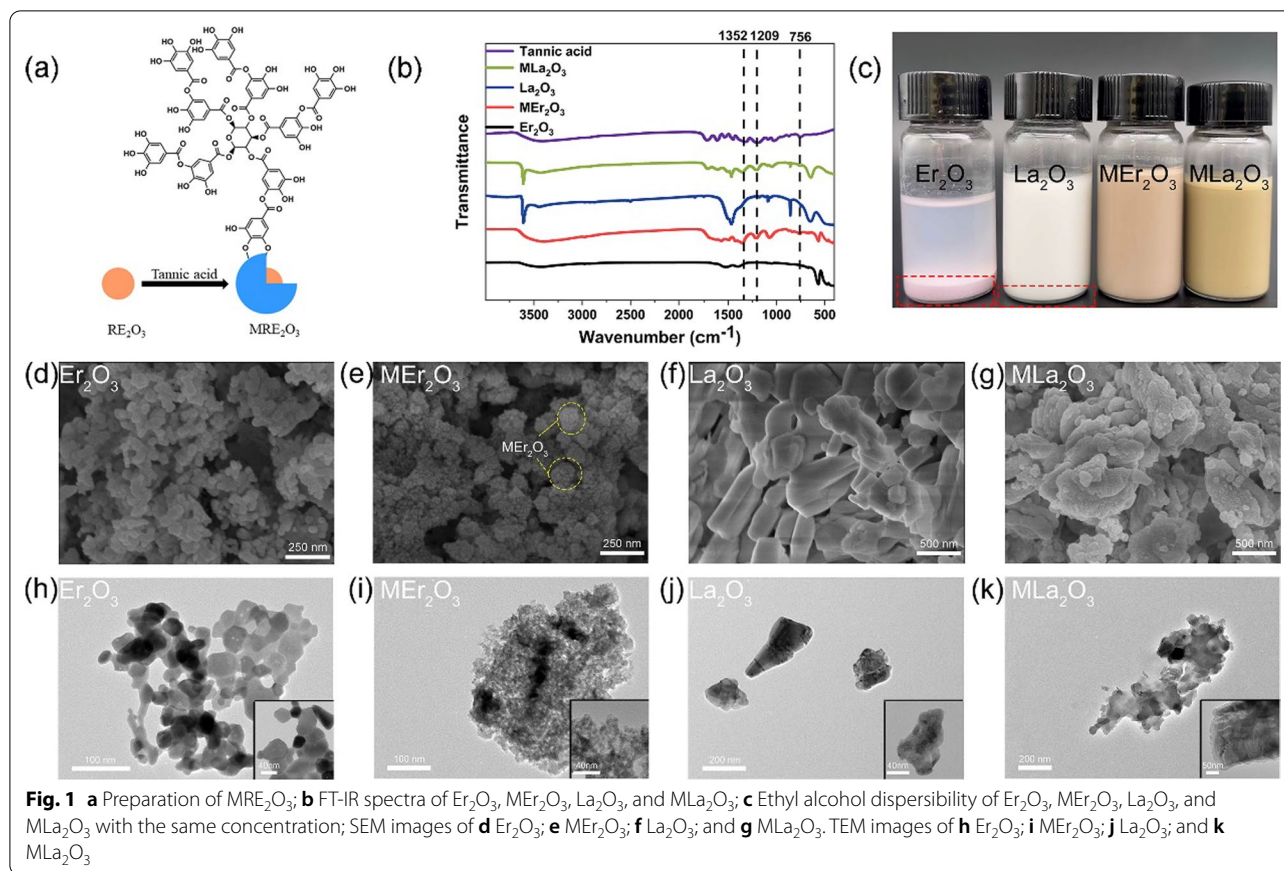## 3 Results and discussion
3.1 Characterization
3.1.1 Characterization of MRE_2O_3
A good particle distribution contributes to the high probability of the attenuation of incident gamma photons [19–21]. Ultra-disperse particles allow the coherent scattering of gamma-ray, subsequently, gamma rays are more attenuated by coherent scattering but not by photoelectric absorption and Compton scattering [22]. Ultra-disperse nano-particles facilitate subsequent spraying operations, and coating will be flatter. Tannic acid was used to modify nanoparticles to decline agglomeration because of its remarkable effect on the dispersion and migration of nanomaterials in aqueous environments (Fig. 1a) [23, 24]. The organic layer formation of MRE_2O_3 is shown in the FT-IR spectrum (Fig. 1b). The peaks at 756 and 1,352 cm^{-1} are related to the C–H stretching vibration of tannic acid, and the peak at 1,209 cm^{-1} is ascribed to the vibration of C=O stretching in tannic acid [25, 26]. In comparison with RE_2O_3, the characteristic peaks of tannic acid were observed for MRE_2O_3, suggesting that tannic acid has successfully attached on the surface of RE_2O_3 and can greatly avoid the aggregation of RE_2O_3 nano particles. Figure 1c shows the dispersion of unmodified nanoparticles and tannic acid modified nanoparticles in 10 wt.% ethyl alcohol at the same concentration. Obviously, Er_2O_3 and Bi_2O_3 nanoparticles settled at the bottom of the bottle via agglomeration. However, MRE_2O_3 shows a high degree of dispersion. Considering the presence of the galloyl groups, many strongly chelating metal ions interact with tannic acid to form a five-member ring [27]. Besides, MRE_2O_3 can be fixed on natural leather because of the excellent adhesion ability of tannic acid for most surface. Figure 1d–g shows the scanning microscopy (SEM) images of RE_2O_3 and MRE_2O_3. The surface morphology of Er_2O_3 tends to be spherical, while that of La_2O_3 is irregular columnar (Fig. 1d, f). The modified rare earth nanoparticles (MRE_2O_3) have rougher surfaces than before (Fig. 1e, g), showing raised spots over nanoparticles. Moreover, RE_2O_3 has greatly changed the microscopic appearance compared with the images of MRE_2O_3 obtained by TEM (Fig. 1h–k). The tannic acid film formed at the surface of RE_2O_3.

3.1.2 Characterization of RZ-NL
Field emission SEM revealed that NL contains the unique D-bands structure of collagen fiber (Fig. 2a). After impregnation of high-Z elements, the D-bands disappeared, and the diameter of fiber increased. Therefore, high-Z elements have been successfully loaded on collagen fiber (Fig. 2a–c). Moreover, Fig. 2b, c show that Bi and Ba were evenly attached on the surface of collagen

Shen *et al. Journal of Leather Science and Engineering* (2022) 4:15

Page 5 of 11

Fig. 1 **a** Preparation of MRE_2O_3; **b** FT-IR spectra of Er_2O_3, MEr_2O_3, La_2O_3, and MLa_2O_3; **c** Ethyl alcohol dispersibility of Er_2O_3, MEr_2O_3, La_2O_3, and MLa_2O_3 with the same concentration; SEM images of **d** Er_2O_3; **e** MEr_2O_3; **f** La_2O_3; and **g** MLa_2O_3. TEM images of **h** Er_2O_3; **i** MEr_2O_3; **j** La_2O_3; and **k** MLa_2O_3

fibers, and the hierarchical structure of the collagen fiber was preserved. Furthermore, the MRE_2O_3 coating and Z_x-NL substrate were observed on a macroscopic level (Fig. 2d–g). Collagen fibers contain many functional groups such as –COOH, –NH$_2$ and –CONH$_2$. These groups make it easy for NL to combine and stabilize many metal ions [28]. The high-Z elements with uniform dispersion on collagen fiber plays a significant role in promoting the probability of collision of gamma photons, leading to the effective attenuation of photons energy.

3.2 Gamma-ray attenuation evaluation of RZ-NL
We coated high Z-natural leather (Z-NL) with rare earth nanoparticles to further attenuate and absorb gamma-ray energy. As shown in Fig. 3a, the protection performance of NL against gamma-ray is very limited, and its shielding efficiency is less than 2%. In comparison with Z_x-NL, the gamma-ray shielding abilities of Er_yZ_x-NL were remarkably improved under the presence of MEr_2O_3 coating. For instance, the attenuation efficiency of $Er_{1.31}Bi_{5.46}$-NL had been increased up to 1.5 times when compared to that of $Bi_{5.46}$-NL in incident of 59.6 keV. The multilayered structure of coating and NL facilitated the occurrence of photoelectric effect in several places within the composites

[29]. The essence of the photoelectric effect lies in the collision between incident gamma photons and particles through which gamma photons attenuate their energy. In the condition, the more atoms collide with the photons, the more the energy of the photons decays. The high-Z elements are uniformly dispersed at the microscopic level, resulting in high electron density and absorbability of gamma rays, and contributing to the attenuation of photons energy [30, 31]. Besides, the energy generated by gamma-ray source deeply affects the absorption of prepared materials, which declines sharply with raising gamma-ray energy. This finding was obtained, because the absorption ability of composite materials is inversely proportional to the cube of gamma-ray energy.

Figure 3a–e shows the gamma-ray attenuation efficiency of RZ-NL substrates with different thicknesses and contents of rare earth elements. It can be observed that the shielding performances of RZ-NL were enhanced by increasing the contents of rare earth element and the thicknesses. These results are attributed to the enhanced photons collision probability by the increase in the number of high-Z elements in the incident path of gamma photons. In general, the photons energy attenuation efficiency of shielding materials could be increased just by
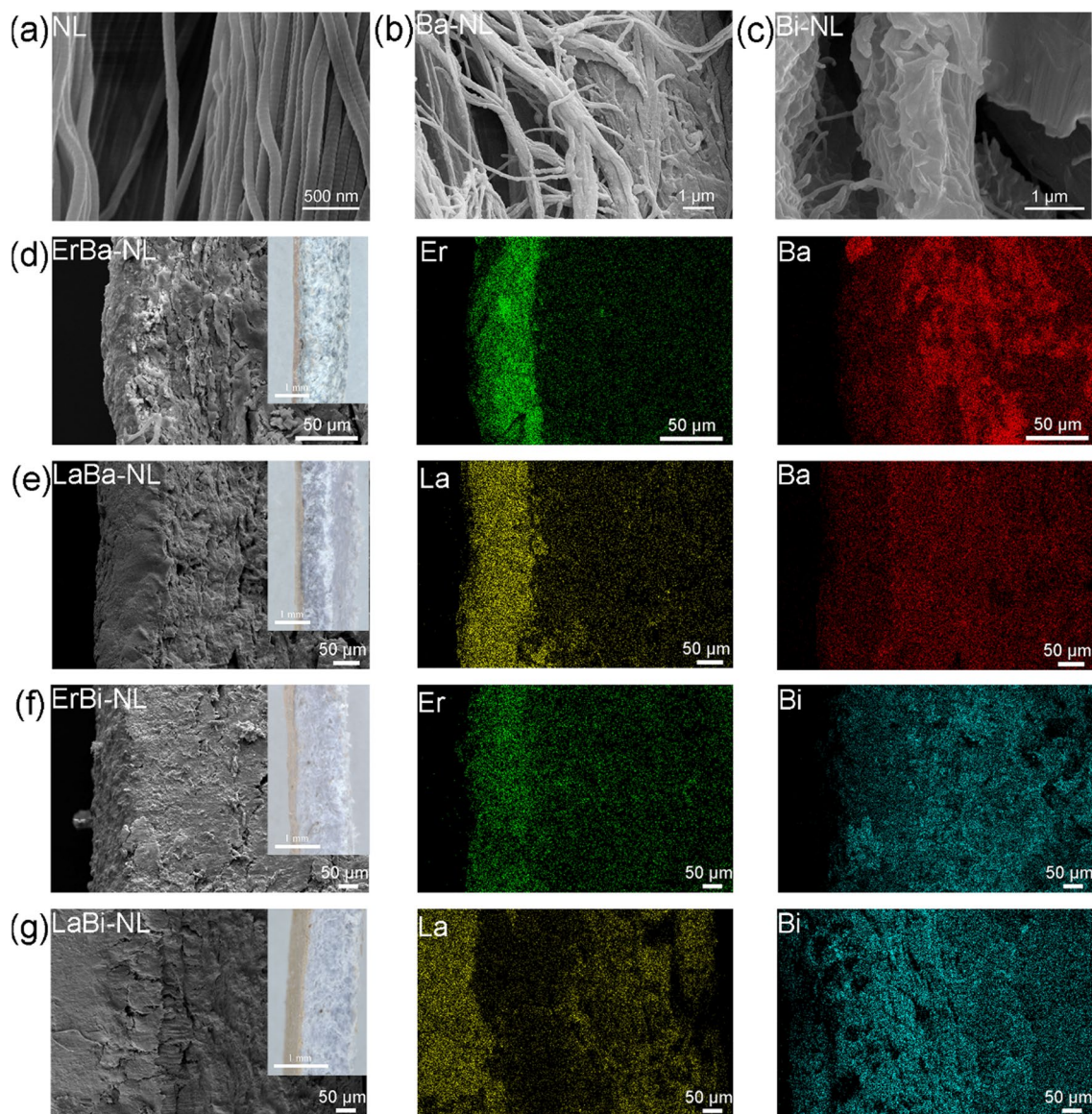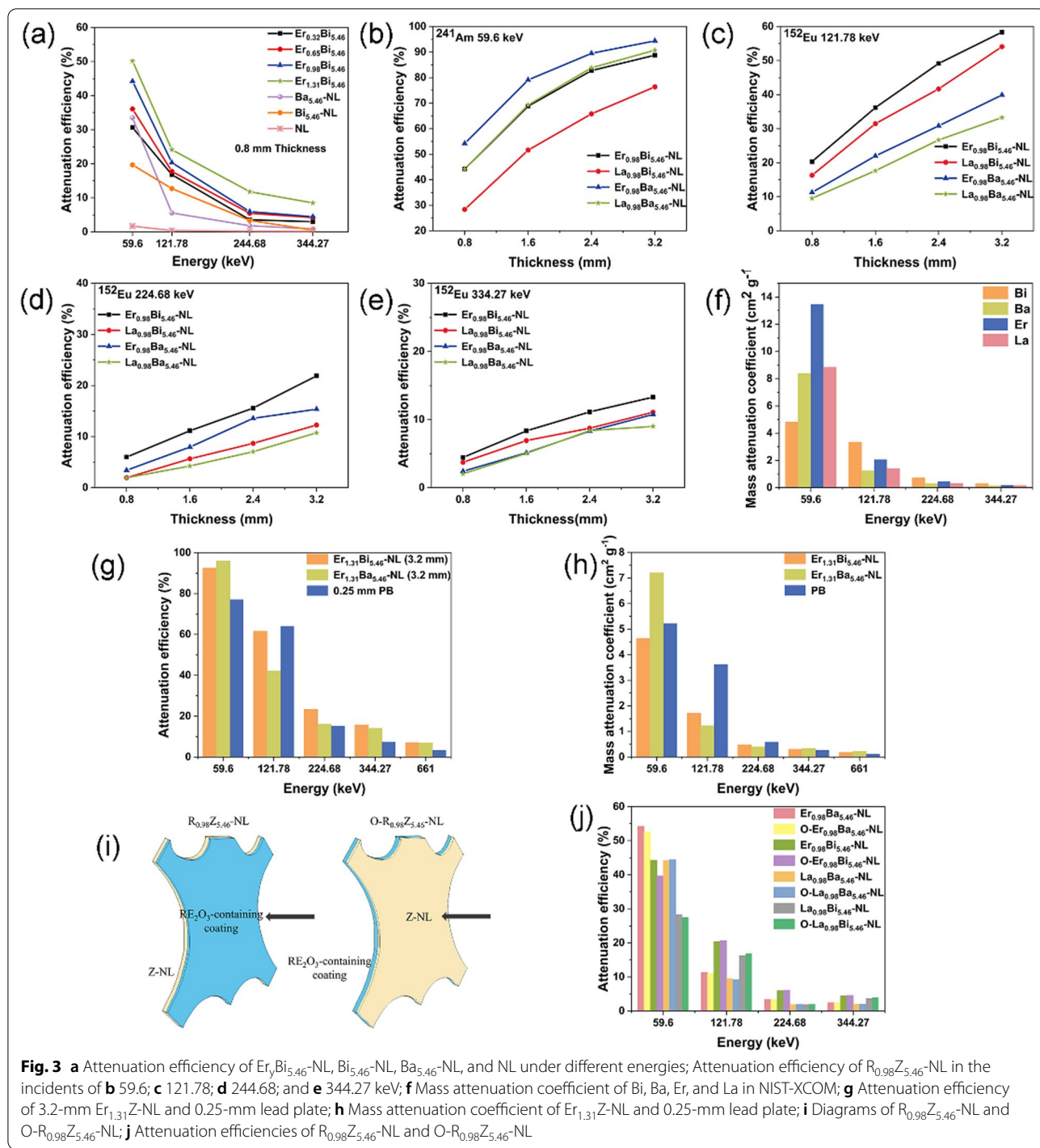
Fig. 2 SEM images and stereoscope photos of **a** NL; **b** $Ba_{5.46}$-NL; **c** $Bi_{5.46}$-NL; Cross-sectional SEM and Mapping images of **d** $Er_{0.32}Ba_{5.46}$-NL; **e** $La_{0.32}Ba_{5.46}$-NL; **f** $Er_{0.32}Bi_{5.46}$-NL; and **g** $La_{0.32}Bi_{5.46}$-NL

increasing their thickness, such as concrete and glass [32, 33]. The ability of composite materials to attenuate gamma-ray energy is not only associated with the atomic number and the incident energy, but also depends on the absorption edge of high-Z elements (often called K absorption edge). When the energy of the gamma rays is close to the absorption edge of the K shell, the probability of photoelectric effect interacted between high-Z element and photons increases [34], resulting higher attenuation efficiency of photons energy. As shown in Fig. 3b–e, it was found that $R_yBa_{5.46}$-NL performs better protection against gamma rays than $R_yBi_{5.46}$-NL (in the same rare earth elements and content) in the incident of 59.6 keV, due to the fact that the K absorption edge of Ba (37.44 keV) is closer to 59.6 keV than that of Bi (90.05 keV). In case of incident of 121.78, 224.68, and 334.27 keV, $R_yBi_{5.46}$-NL exhibited more effective than that of $R_yBa_{5.46}$-NL, because the K absorption edge of Bi is more closed to the gamma energy. Compared La and Er, their adsorption edges are 38.92 and 57.49 keV respectively, therefore, the ability of $Er_yZ_{5.46}$-NL to attenuate gamma rays is better than $La_yZ_{5.46}$-NL (in the same high Z elements and content) in the incident of 59.6–334.27 keV due to the K absorption edge of Er is more

Fig. 3 a Attenuation efficiency of $Er_yBi_{5.46}$-NL, $Bi_{5.46}$-NL, $Ba_{5.46}$-NL, and NL under different energies; Attenuation efficiency of $R_{0.98}Z_{5.46}$-NL in the incidents of **b** 59.6; **c** 121.78; **d** 244.68; and **e** 344.27 keV; **f** Mass attenuation coefficient of Bi, Ba, Er, and La in NIST-XCOM; **g** Attenuation efficiency of 3.2-mm $Er_{1.31}Z$-NL and 0.25-mm lead plate; **h** Mass attenuation coefficient of $Er_{1.31}Z$-NL and 0.25-mm lead plate; **i** Diagrams of $R_{0.98}Z_{5.46}$-NL and O-$R_{0.98}Z_{5.46}$-NL; **j** Attenuation efficiencies of $R_{0.98}Z_{5.46}$-NL and O-$R_{0.98}Z_{5.46}$-NL

closed to the incident gamma photons. On the other hand, the mass attenuation coefficient in NIST-XCOM (Fig. 3f) indicates that the mass attenuation coefficient of Bi (4.82 cm^2 g^{-1}) is lower than that of Ba (8.39 cm^2 g^{-1}) in the incident of 59.6 keV. By contrast, the mass attenuation coefficient of Ba is less than that of Bi at 121.78, 244.68, and 334.27 keV. In other words, the attenuation

ability of Bi to gamma-ray energy is weaker than that of Ba in the incident of 59.6 keV. Meanwhile, at the incident of 121.78 keV and higher gamma-ray energy, the attenuation ability of Bi is higher than that of Ba because of its higher mass attenuation coefficient. $Er_yBi_{5.46}$-NL and $La_yBi_{5.46}$-NL also exhibited different ability to attenuate gamma rays energy. The mass attenuation efficient

of erbium (Er) is higher than that of lanthanum (La) in NIST-XCOM (Fig. 3f). Therefore, the performance of $Er_{0.98}Ba_{5.46}$-NL is superior to that of $La_{0.98}Ba_{5.46}$-NL in terms of attenuating gamma rays energy.

The attenuation efficiency and mass attenuation efficient of $Er_{1.31}Z_{5.46}$-NL and lead plate (PB) are presented in Fig. 3g, h. The attenuation efficiency of $Er_{1.31}Ba_{5.46}$-NL at a thickness of 3.2 mm reached 96.4% in the incident of 59.6 keV and decreased to 61.57% in the incident of 121.78. Moreover, the attenuation ability of $Er_{1.31}Z_{5.46}$-NL is superior to that of lead plate (PB) in the incident of 59.6, 224.68, 334.27, and 661 keV compared with the 0.25 mm-lead plate (54.54 mmol cm^{-3}), as shown in Fig. 3g. In addition, the mass attenuation coefficient of $Er_{1.31}Ba_{5.46}$-NL (7.21 $cm^2 g^{-1}$) is greatly higher than that of 0.25-mm PB in the incident of 59.6 keV (5.22 $cm^2 g^{-1}$), suggesting the advantages of RZ-NL in the attenuation of relative low gamma-ray energy. However, the attenuation abilities of RZ-NL and PB against gamma-ray are limited at higher energy, especially when the energy is higher than 344.27 keV. The attenuation efficiency of $Er_{1.31}Bi_{5.46}$-NL is 14.03% in incident of 334.27 keV, while that is only 6.88% in incident of 661 keV (^{137}Cs). Therefore, the effective attenuation of high gamma rays energy is still a challenge.
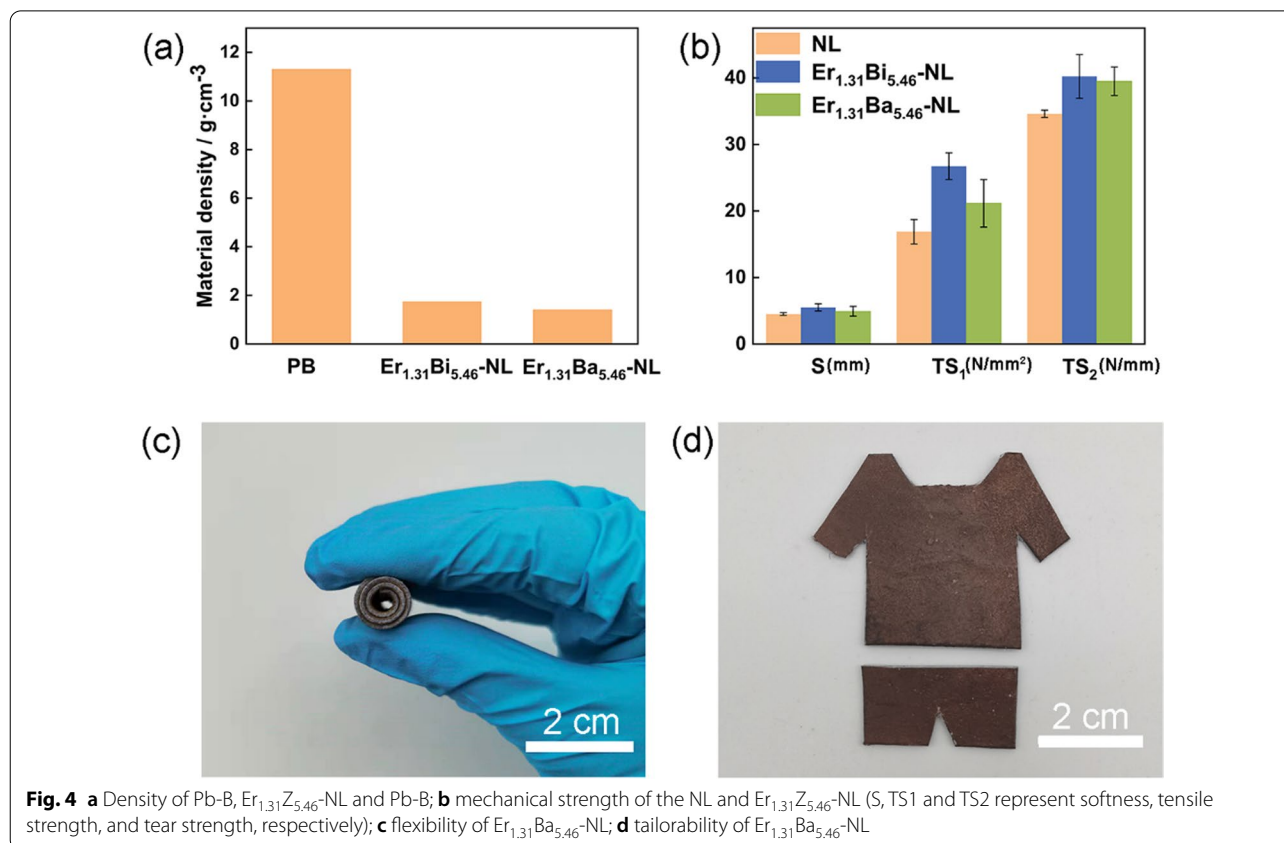
In addition, the combination of different high-Z elements may exhibit different attenuation behaviors. Accordingly, we designed an experiment in which gamma rays were first irradiated with $Z_{5.46}$-NL layer and then to coating layer (RE_2O_3), which was denoted as O-$R_{0.98}Z_{5.46}$-NL (Fig. 3i). Figure 3j shows the attenuation behaviors of $R_{0.98}Z_{5.46}$-NL and O-$R_{0.98}Z_{5.46}$-NL at different incident of gamma rays. The low gamma rays energy (59.6 keV) was effective for $Er_{0.98}Bi_{5.46}$-NL,

because the fact that the K absorption edge of Er is 57.49 keV, which very close to 59.6 keV than that of Bi (90.05 keV, K absorption edge). Under high gamma rays energy, O-$Er_{0.98}Bi_{5.46}$-NL is more effective. After first attenuated by Bi, the energy of photons was reduced and may be located in the optimal attenuation range of Er. Theoretically, for the photons with higher energy, their energy will be reduced after first collide with high Z element and should be more effective attenuated further by the element with relative low K adsorption edge. On the other hand, the high Z elements with high K adsorption edge are often heavy than that of elements with low K adsorption edge, such as Bi and Ba, Bi and La. In order to reduce the weight and more effectiveness of shielding materials, it is reasonable to use the combination of high Z elements with different K adsorption edge. Therefore, gamma rays with high energy should be first attenuated by the elements with high K absorption edge and then by the elements with relative low K absorption edge.

Our previous investigations are focused on the development of X-ray shielding materials based on natural leather [28, 31]. In this work, the high Z elements impregnated natural leather with nano RE_2O_3 coating will be prepared and their gamma rays shielding materials energy attenuation performances were investigated. In comparison, the attenuation efficiency of natural leather based shielding materials used for the energy attenuation of X-ray and gamma-ray are summarized in Table 1. It can be observed that the natural leather based shielding materials are effective for the X-rays and gamma-ray energy attenuation, but this ability is greatly related with high Z element dosage and species, thickness and structure.

Table 1 The attenuation efficiency of natural leather based shielding materials used for X-ray and Gamma-ray

No.	High Z elements and content	Thickness	X-ray or Gamma-ray and energy	Attenuation efficiency (%)	References
1	Nano Bi_2O_3, 1.51 mmol cm^{-3} Dispersed in leather	1.4 mm	X-ray, 48 keV	58.0	[28]
			X-ray, 65 keV	40.0	[28]
			X-ray, 83 keV	32.0	[28]
2	Nano Ce_2O_3, 1.51 mmol cm^{-3} Dispersed in leather	1.4 mm	X-ray, 48 keV	35.0	[28]
			X-ray, 65 keV	42.0	[28]
			X-ray, 83 keV	58.0	[28]
3	Bi^{3+}, 0.96 mmol cm^{-3} I^-, 6.89 mmol cm^{-3} Dispersed in leather by coordination	1.0 mm	X-ray, 48 keV	92.0	[31]
			X-ray, 65 keV	81.3	[31]
			X-ray, 83 keV	65.8	[31]
4	Bi^{2+}, 5.46 mmol cm^{-3} Nano Er_2O_3, 1.31 mmol cm^{-3} Bi^{2+} was dispersed in leather by coordination Nano Er_2O_3 coated on the surface of leather	3.2 mm	Gamma-ray, ^{241}Am, 59.6 keV	92.49	This work
			Gamma-ray, ^{152}Eu, 121.78 keV	61.57	This work

Shen *et al. Journal of Leather Science and Engineering* (2022) 4:15

Page 9 of 11

Fig. 4 **a** Density of Pb-B, $Er_{1.31}Z_{5.46}$-NL and Pb-B; **b** mechanical strength of the NL and $Er_{1.31}Z_{5.46}$-NL (S, TS1 and TS2 represent softness, tensile strength, and tear strength, respectively); **c** flexibility of $Er_{1.31}Ba_{5.46}$-NL; **d** tailorability of $Er_{1.31}Ba_{5.46}$-NL

3.3 Mechanical properties of RZ-NL

Natural leather takes the advantages of being soft and suitable for wearing. We conducted detailed tests on its physical properties of RZ-NL. As shown in Fig. 4a, the density of $Er_{1.31}Ba_{5.46}$-NL is only 1.4 g cm^{-3}, which is only 1/8 of lead plate (11.3 g cm^{-3}). In addition, the tensile strength (TS_1) of $Er_{1.31}Bi_{5.46}$-NL and $Er_{1.31}Ba_{5.46}$-NL were 26.75 and 21.16 N mm^{-2}. The tear strength (TS_2) of $Er_{1.31}Bi_{5.46}$-NL and $Er_{1.31}Ba_{5.46}$-NL were 40.23 and 39.51 N mm^{-1}, respectively. RZ-NL exhibited outstanding mechanical strength, which are somewhat higher than that of NL because of the crosslinking effect of high-Z elements. Besides, RZ-NL exhibits excellent softness (S), flexibility, and tailorability as natural leather (NL), as shown Fig. 4c–d. Furthermore, it was found that the attenuation efficiency of prepared gamma-ray materials was decreased within 5% after 20,000 times crimping, suggesting excellent bending resistance. Our previous work shown that the natural leather based X-ray shielding materials exhibited superb stability after bending 29,000 times [35].

4 Conclusion

Novel gamma rays shielding composites (RZ-NL) based on natural leather were prepared using equivalent-volume impregnation and coating approaches. Results that the high-Z elements were uniformly dispersed because of the active groups in natural leather, which enhanced the attenuation of photons energy. The aggregation problem of rare earth nano-particles (RE_2O_3) was effectively solved using tannic acid, and RE_2O_3 was easily coated on the surface of natural leather. The prepared RZ-NL exhibited outstanding attenuation ability of gamma rays, especially in the incident of 59.6 keV (^{241}Am), which can be comparable with 0.25 mm Pb. Further investigation indicated that the gamma rays with higher energy can be effectively attenuated by first attenuating it with elements having high K absorption edge and then by elements with relative low K absorption edge. In addition, RZ-NL exhibited excellent mechanical strength, softness, flexibility, and tailorability as natural leather.

Author contributions

XL and YS designed the research. YS and JZ performed the experiment and analyzed the data. XL, YS and JZ wrote the manuscript. All the authors have given approval to the final version of the manuscript.

Availability of data and materials

All data from this study are presented in the paper.

Declarations

Competing interests

The authors declare no competing financial interest.

Author details

[1]Department of Biomass Science and Engineering, Chengdu 610065, China. [2]The Key Laboratory of Leather Chemistry and Engineering of Ministry of Education, Sichuan University, Chengdu 610065, China. [3]Institute of Nuclear Science and Technology, Sichuan University, Chengdu 610065, China.

References

1. Azencott R, Chalmond B, Coldefy F. Association of adaptative smoothing and markovian models for detection of valley bottoms on strongly noisy images (nondestructive testing). In: Proceedings, 11th IAPR international conference on pattern recognition, vol IV. Conference D: architectures for vision and pattern recognition. IEEE Comput. 1992, pp. 327–330. https://doi.org/10.1109/ICPR.1992.201991

2. Lees JE, Bassford DJ, Blake OE, Blackshaw PE, Perkins AC. A hybrid camera for simultaneous imaging of gamma and optical photons. J Instrum. 2012;7:6009–6009. https://doi.org/10.1088/1748-0221/7/06/P06009.

3. Liu R, Shi J, Ge X, Yang BT, Zhang H, Zhang JX, Ma JM. Similar therapeutic effects of 125I seed radiotherapy and γ-ray radiotherapy on lacrimal gland adenoid cystic carcinoma. Int J Ophthalmol. 2021;14:547–53. https://doi.org/10.18240/ijo.2021.04.11.

4. Thabet NM, Mohamed K, Abdel R, Moustafa EM, Comsan MNH. Boswellic acid protects against bisphenol-a and gamma radiation induced hepatic steatosis and cardiac remodelling in rats: role of hepatic PPAR-α/P38 and cardiac calcineurin-A/NFATc1/P38 pathways. Arch Physiol Biochem. 2020. https://doi.org/10.1080/13813455.2020.1727526.

5. El-Sharkawy RM, Allam EA, El-Taher A, Elsaman R, El Sayed ME, Mahmoud ME. Synergistic effects on gamma-ray shielding by novel light-weight nanocomposite materials of bentonite containing nano Bi2O3 additive. Ceram Int. 2021. https://doi.org/10.1016/j.ceramint.2021.11.290.

6. Rezaei-Ochbelagh D, Azimkhani S. Investigation of gamma-ray shielding properties of concrete containing different percentages of lead. Appl Radiat Isot. 2012;70:2282–6. https://doi.org/10.1016/j.apradiso.2012.06.020.

7. Obaid SS, Gaikwad DK, Pawar PP. Determination of gamma rays shielding parameters of rocks and concrete. Radiat Phys Chem. 2018;144:356–260. https://doi.org/10.1016/j.radphyschem.2017.09.022.

8. Kaur P, Singh K, Thakur S, Singh P, Bajwa B. Investigation of bismuth borate glass system modified with barium for structural and gamma-ray shielding properties. Spectroc Acta A-Molec Biomolec Spectr. 2019;26:367–77. https://doi.org/10.1016/j.saa.2018.08.038.

9. Soni BK, Makwana R, Mukherjee S, Barala SS, Parashari S, Chauhan R, Jodha AS, Katovsky K. Novel concrete compositions for γ-rays and neutron shielding using WC and B4C. Results Mater. 2021;10: 100177. https://doi.org/10.1016/j.rinma.2021.100177.

10. Khalaf MA, Ban CC, Ramli M, Ahmed NM, Sern LJ, Khaleel HA. Physicomechanical and gamma-ray shielding properties of high-strength heavyweight concrete containing steel furnace slag aggregate. J Build Eng. 2020;30: 101306. https://doi.org/10.1016/j.jobe.2020.101306.

11. Laariedh F, Prabhu NS, Sayyed MI, Kumar A, Alfadhli S, Kamath SD. Impact of replacement of B2O3 by TeO2 on the physical, optical and gamma rays shielding characteristics of Pb-free B2O3-TeO2-ZnO-Al2O3-Li2O-MgO glass system. Optik. 2021;248: 168100. https://doi.org/10.1016/j.ijleo.2021.168100.

12. Alotaibi BM, Alotiby M, Kumar A, Mahmoud KA, Sayyed MI, Al-Yousef HA, Al-Hadeethi Y. Gamma-ray shielding, physical, and structural characteristics of TeO2–CdO–PbO–B2O3 glasses. Opt Mater. 2021;119: 111333. https://doi.org/10.1016/j.optmat.2021.111333.

13. Billen P, Leccisi E, Dastidar S, Li S, Lobaton L, Spatari S, Fafarman AT, Fthenakis VM, Baxter JB. Comparative evaluation of lead emissions and toxicity potential in the life cycle of lead halide perovskite photovoltaics. Energy. 2019;166:1089–96. https://doi.org/10.1016/j.energy.2018.10.141.

14. Ahmed B, Shah GB, Malik AH, Aurangzeb RM. Gamma-ray shielding characteristics of flexible silicone tungsten composites. Appl Radiat Isot. 2020;155:108901. https://doi.org/10.1016/j.apradiso.2019.108901.

15. Canel A, Korkut H, Korkut T. Improving neutron and gamma flexible shielding by adding medium-heavy metal powder to epoxy based composite materials. Radiat Phys Chem. 2019;158:13–6. https://doi.org/10.1016/j.radphyschem.2019.01.005.

16. Li H, Zheng W, Xiao H, Hao B, Wang Y, Huang X, Shi B. Collagen fiber membrane-derived chemically and mechanically durable superhydrophobic membrane for high-performance emulsion separation. J Leather Sci Eng. 2021;3:20. https://doi.org/10.1186/s42825-021-00060-5.

17. Luo F, Zhong X, Gao M, Peng B, Long Z. Progress and mechanism of breaking glycoconjugates by glycosidases in skin for promoting unhairing and fiber opening-up in leather manufacture. A Review J Leather Sci Eng. 2020;2:12. https://doi.org/10.1186/s42825-020-00025-0.

18. Liu C, Wang X, Huang X, Liao X, Shi B. Absorption and reflection contributions to the high performance of electromagnetic waves shielding materials fabricated by compositing leather matrix with metal nanoparticles. ACS Appl Mater Interfaces. 2018;10:14036–44. https://doi.org/10.1021/acsami.8b01562.

19. Tiamduangtawan P, Kamkaew C, Kuntonwatchara S, Wimolmala E, Saenboonruang K. Comparative mechanical, self-healing, and gamma attenuation properties of PVA hydrogels containing either nano- or micro-sized Bi2O3 for use as gamma-shielding materials. Radiat Phys Chem. 2020;177: 109164. https://doi.org/10.1016/j.radphyschem.2020.109164.

20. Elsafi M, Dib MF, Mustafa HE, Sayyed MI, Khandaker MU, Alsubaie A, Almalki ASA, Abbas MI, El-Khatib AM. Enhancement of ceramics based red-clay by bulk and nano metal oxides for photon shielding features. Materials. 2021;14:7878. https://doi.org/10.3390/ma14247878.

21. Kim Y, Park S, Seo Y. Enhanced X-ray shielding ability of polymer-non-leaded metal composites by multilayer structuring. Ind Eng Chem Res. 2015;54:5968–73. https://doi.org/10.1021/acs.iecr.5b00425.

22. Li R, Gu Y, Wang Y, Yang Z, Li M, Zhang Z. Effect of particle size on gamma radiation shielding property of gadolinium oxide dispersed epoxy resin matrix composite. Mater Res Express. 2017;4: 035035. https://doi.org/10.1088/2053-1591/aa6651.

23. Pan D, Zhang X, Yang G, Shang Y, Su F, Hu Q, Patil RR, Liu H, Liu C, Guo Z. Thermally conductive anticorrosive epoxy nanocomposites with tannic acid-modified boron nitride nanosheets. Ind Eng Chem Res. 2020;59:20371–81. https://doi.org/10.1021/acs.iecr.0c04510.

24. Wang JQ, Lou TJ, Wang T, Cao W, Zhao H, Qian PF, Bao ZL, Yuan XT, Geng HZ. Flexible electrothermal laminate films based on tannic acid-modified

carbon nanotube/thermoplastic polyurethane composite. Ind Eng Chem Res. 2021;60:7844–52. https://doi.org/10.1021/acs.iecr.1c00964.

25. Yin L, Mi N, Yao Y, Li J, Zhang Y, Yang S, He H, Hu X, Li S, Ni L. Efficient removal of Cr(VI) by tannic acid-modified FeS nanoparticles: performance and mechanisms. Water Sci Eng. 2021;14:210–8. https://doi.org/10.1016/j.wse.2021.08.006.

26. Saniei N, Ghasemi N, Zinatizadeh AA, Zinadini S, Ramezani M, Derakhshan AA. Electricity generation enhancement in microbial fuel cell via employing a new SPEEK based proton exchange membrane modified by goethite nanoparticles functionalized with tannic acid and sulfanilic acid. Environ Technol Innov. 2022;25: 102168. https://doi.org/10.1016/j.eti.2021.102168.

27. Xiong LL, Huang R, Chai HH, Yu L, Li CM. Facile synthesis of Fe 3O4@ tannic acid@au nanocomposites as a catalyst for 4-nitrophenol and methylene blue removal. ACS Omega. 2020;5:20903–11. https://doi.org/10.1021/acsomega.0c02347.

28. Li Q, Wang Y, Xiao X, Zhong R, Liao J, Guo J, Liao X, Shi B. Research on X-ray shielding performance of wearable Bi/Ce-natural leather composite materials. J Hazard Mater. 2020;398: 122943. https://doi.org/10.1016/j.jhazmat.2020.122943.

29. Li Z, Zhou W, Zhang X, Gao Y, Guo S. High-efficiency, flexibility and lead-free X-ray shielding multilayered polymer composites: layered structure design and shielding mechanism. Sci Rep. 2021;11:4384. https://doi.org/10.1038/s41598-021-83031-4.

30. Mahmoud ME, El-Khatib AM, Halbas AM, El-Sharkawy RM. Ceramic tiles doped with lead oxide nanoparticles: their fabrication, physical, mechanical characteristics and γ-ray shielding performance. Radiat Phys Chem. 2021;189: 109780. https://doi.org/10.1016/j.radphyschem.2021.109780.

31. Wang Y, Ding P, Xu H, Li Q, Guo J, Liao X, Shi B. Advanced X-ray shielding materials enabled by the coordination of well-dispersed high atomic number elements in natural leather. ACS Appl Mater Interfaces. 2020;12:19916–26. https://doi.org/10.1021/acsami.0c01663.

32. Kumar A. Gamma rays shielding properties of PbO-Li2O-B2O3 glasses. Radiat Phys Chem. 2017;136:50–3. https://doi.org/10.1016/j.radphyschem.2017.03.023.

33. Sayyed MI, Tekin HO, Kılıcoglu O, Agar A, Zaid MHM. Shielding features of concrete types containing sepiolite mineral: Comprehensive study on experimental, XCOM and MCNPX results. Results Phys. 2018;11:40–5. https://doi.org/10.1016/j.rinp.2018.08.029.

34. Lim TY, Wagiran H, Hussin R, Hashim S. Mass attenuation coefficients and effective atomic numbers of strontium borate glass system in the energy range 0.01- 1.25 MeV. Adv Mater Res. 2014;895:315–8. https://doi.org/10.4028/www.scientific.net/AMR.895.315.

35. Li Q, Ding P, Wang Y, Liao X, Shi B. Preparation of a rare earth natural leather X-ray protection material and its properties. Acta Phys-Chim Sin. 2021;37:2001046. https://doi.org/10.3866/PKU.WHXB202001046.

Publisher's Note